not entirely Maxwellian. The transition probability decreases to about 50 percent at high rf amplitudes but more slowly than would be expected for a rectangular pulse. It is remarkable that, in some cases, an increase of the transition probability to as much as 75 percent is observed at very high rf amplitudes. The effects depend markedly on the details of the rf circuit.

The dc field in which the transitions are observed is so constructed that the occurrence of significant inhomogeneities is unlikely. Further, for at least some rf circuits, the lines are highly symmetrical at rf amplitudes much greater than those required to give width saturation. Generally, it is to be expected that the use of the high rf amplitudes in a nonuniform magnetic field would give rise to anomalously large line widths, distorted line shapes, and possibly relatively large shifts in line frequency. Since the effects here under consideration do not show these features, it is unlikely that a field inhomogeneity is responsible for them.

Because of the great dependence of the details of the effect on the structure of the rf circuit and its shield, it seems probable that the effects arise within the portion of the path of the atom in which the amplitude changes between its maximum value and zero. Presumably the adiabatic traverse of the atom over the region in which an end effect occurs, reduces the probability of transition to a vanishingly small value for frequencies at which transitions would occur for a rectangular rf pulse. The effects are not, however, understood in detail and no explanation is offered for the relative constancy of the line frequency as the amplitude is increased and for the high probability of transition occasionally observed for very high rf amplitude.

ACKNOWLEDGMENTS

I wish to thank Mr. Harold Salwen for instructive discussions of these experiments. Mr. Thomas Eck gave extensive aid in taking the data of these experiments.

PHYSICAL REVIEW VOLUME 101, NUMBER 2 JANUARY 15, 1956

Elastic Scattering of 48-Mev Alpha Particles*

R. E. Ellis and Larry Schecter†
Radiation Laboratory, University of California, Berkeley, California
(Received August 25, 1955)

The angular distributions of alpha particles scattered elastically from Ag, Au, and Pb targets have been measured. Deviations by three to four orders of magnitude from pure Coulomb scattering have been observed beyond the forward angles. In addition, some regular structure appears in these distributions, but the main features can be described by an exponential falloff between 25° and 90°.

By fitting the data with a simple modification of Blair's scattering theory, it has been possible to determine interaction radii. Nuclear radii have been derived which are in agreement with those found from medium-energy nucleon scattering.

I. INTRODUCTION

RECENTLY, in order to explain the variation of alpha-particle elastic scattering with energy,[1] Blair[2] proposed a semiclassical scattering model which requires only the use of the well-known phase shifts that appear in the Coulomb interaction. Assuming a well-defined radius for both the target nucleus and the incident alpha particle, he derives the following angular distribution for elastically scattered alpha particles, relative to pure Coulomb scattering,

$$\frac{\sigma}{\sigma_c}=\left|-i\exp[-in\ln\sin^2(\theta/2)]-\frac{\sin^2(\theta/2)}{n}\times\sum_{l=0}^{l'}(2l+1)W_l e^{2i(\delta_l-\delta_0)}P_l(\cos\theta)\right|^2, \quad (1)$$

where l' satisfies the relation

$$l'(l'+1)=(E-E_c)2MR^2/\hbar^2, \quad (2)$$

with $E_c=ZZ'e^2/R$. Here l' is the orbital angular momentum of a particle of mass M, energy E, and velocity v; E_c is the Coulomb energy at the classical turning point; R is the sum of target radius and alpha-particle radius; Ze is the charge of the target nucleus and $Z'e$ is the charge of the alpha particle; and W_l is the weight given to the absorption of the lth partial wave. The Coulomb phases obey the relation

$$e^{2i(\delta_l-\delta_0)}=\frac{l+in}{l-in}e^{2i(\delta_{l-1}-\delta_0)},$$

$$n=ZZ'e^2/\hbar v.$$

The first term in Eq. (1) represents the Coulomb scattering amplitude, and the second term the interaction with the nucleus, of alpha particles with $l\leqq l'$. Blair assumes that all these partial waves with $0\leqq l\leqq l'$ vanish

* This work was done under the auspices of the U. S. Atomic Energy Commission.
† Now at Oregon State College, Corvallis, Oregon.
[1] G. W. Farwell and H. E. Wegner, Phys. Rev. **95**, 1212 (1954).
[2] J. S. Blair, Phys. Rev. **95**, 1218 (1954).

because the trajectory is such that the alpha particle is completely absorbed by the nucleus, excites the nucleus and is lost to elastic scattering, or is broken up into smaller components. Thus $W_l=1$ (complete absorption) for $0\leqq l\leqq l'$. If the nucleus and alpha particle do not overlap, the partial waves associated with the alpha particle are considered to have purely Coulomb phase characteristics; $W_l=0$ (no absorption) for $l>l'$. This model is referred to as the "sharp cut-off" model because complete nuclear absorption ends and complete Coulomb scattering begins at a well-defined distance from the scattering center. The model neglects barrier penetration and reflection from the nuclear potential, and takes no account of the mean free path of the alpha particle in nuclear matter. Although this theory reproduces the general qualitative features of observed angular distributions, namely a rise followed by a sharp falloff, the theoretical curves show a diffraction pattern which is not observed. This last effect is presumably due to the sharp radial cutoff of the Blair theory.

Other investigators[3] have attempted to improve the model in a simple way, by taking $W_l=1$ for $0\leqq l<l'$, $W_l=0.5$ for $l=l'$, and $W_l=0$ for $l>l'$. This "fuzzy" model smooths out the transition region of interaction, and substantially improves the fits to the data at 22 Mev. This fitting results in a determination of the interaction radii, which are found to be larger than the generally accepted values.

Recently, Porter[4] has proposed a classical interpretation of the dependence of the ratio of observed differential cross section to the Coulomb cross section on the classical apsidal distance, D (the distance of closest approach). His description embodies the principle that the scattered intensity, as a function of apsidal distance (and, therefore, of the incident energy and angle of scattering), arises entirely from absorption along the undistorted Coulomb orbit. He defines the ratio of observed to Coulomb cross section in terms of a transmission factor T, which is equal to the fraction of the incident beam that is scattered at a given angle, relative to the Coulomb scattering. T has the form: $T=\exp[-\int dx/l(x)]$, where $l(x)=$mean free path of the alpha particle as a function of the position coordinate x along the path. Assuming straight-line paths through the nucleus, he obtains the expression

$$T=\exp\left(-2\frac{R}{l_0}h[\xi,\delta]\right),$$

where

$$h[\xi,\delta]=\int_\xi^\infty dv(v^2-\xi^2)^{\frac{1}{2}}\operatorname{sech}^2\left(\frac{v-1}{\delta}\right)$$

and $\xi=D/R$, where $R=$interaction radius, the sum of nuclear and alpha-particle radii; $v=r/R$, where $r=$distance from nuclear center to the center of the alpha particle; $\delta=d/R$, where $d=$measure of the thickness of the diffuse edge of the nucleus; $l_0=$mean free path of the alpha particle near the center of the nucleus.

From data previously available[1,3,5] he deduces values of $R/l_0\sim3$ or 4 for alpha particles, $\delta\sim0.2$, and $d\sim2\times10^{-13}$ centimeter, indicating that the nucleus is opaque to alpha particles except near the edge of the nucleus, in the diffuse region. The slight rise of T above unity for small angles, and the structure in the observed distributions which probably arises from wave-mechanical interference effects, are not explained on this model.

Unpublished calculations by Ford and Wheeler[4,5] on the elastic scattering of alpha particles are based on a model in which the "rim" of the nucleus is transparent to the alpha particles. Best agreement between experiment and theory on this model is for large energy and scattering angle for the alpha particle.

Other investigators[1,3,5] have studied elastic alpha-particle scattering, from the point of view of both energy dependence and angular dependence of the cross section. The reported investigations were carried out at somewhat lower energies (13 Mev to 44 Mev) than those reported here. They show a pronounced deviation from Coulomb scattering at relatively small angles of scattering, and the ratio of observed to Coulomb cross section is essentially an exponentially decreasing function of angle over a wide range of angles beyond the point at which the break with Coulomb scattering is observed.

The purpose of the experiments reported here was to extend these investigations, both as to theory and as to experiment. For comparison's sake, the heavy target nuclei of silver, gold, and lead were concentrated on, as it would be interesting to compare the results at higher bombarding energy with those obtained at lower energies.

II. EXPERIMENTAL METHOD

A. General Procedure

A schematic diagram of the experimental arrangement is shown in Fig. 1. The 48-Mev alpha-particle beam of the 60-inch cyclotron at the Crocker Laboratory was brought out through the water shielding and impinged on a target which was located at the center of a large vacuum scattering chamber. The scattered particles were detected by a triple-coincidence proportional counter telescope. At each angular setting of the detector, the number of alpha particles elastically scattered during a convenient time interval was observed with the telescope and normalized against the total charge collected by a Faraday cup located behind the chamber. The detected particles were selected by placing absorbers in front of the counter and requiring a preset minimum pulse height in each counter chamber. In this way, the relative elastic scattering cross section was obtained as a function of the laboratory angle.

[3] Wall, Rees, and Ford, Phys. Rev. **97**, 726 (1955).
[4] C. E. Porter, Phys. Rev. **99**, 1400 (1955).
[5] Wegner, Eisberg, and Igo, Phys. Rev. **99**, 825 (1955).

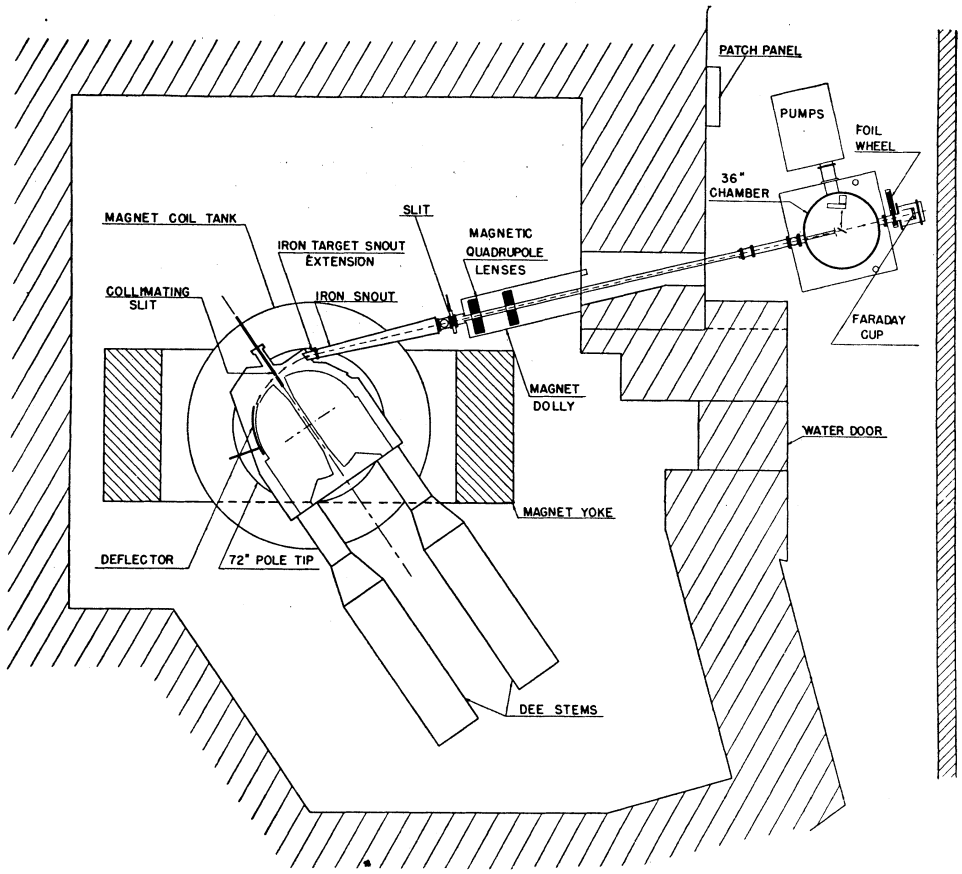

FIG. 1. Schematic diagram of experimental arrangement.

B. Beam Monitoring and Beam Energy Determinations

A cylindrical brass Faraday cup, maintained in a separate vacuum compartment with its own diffusion pump, was located on the beam-exit port of the scattering chamber. Two opposed C-shaped magnets (Alnico III) were located at the rear of the cup and provided a uniform field of about 200 gauss for prevention of secondary electron loss occasioned by the beam's striking the beam-stopping plate. Suitable coaxial leads permitted transmission of the beam current to a 100% negative feedback electrometer located in the counting area.

The precision capacitors used in conjunction with the integrating electrometer were calibrated against precision capacitors of the same nominal values. These in turn have been calibrated against a 1.0-microfarad condenser certified by the Bureau of Standards. Capacitors used in integrating the beam were calibrated for each run and it is believed that their values are correctly known to within one percent. The voltage on the integrating condensers was measured during a run by a Speedomax recorder. The linearity of response of the recorder and electrometer scale factors were checked for each run, and any variation in values thus obtained was taken into account. It is thought that the voltages read from the recorder are accurate to within 0.5%.

Between the scattering chamber and the Faraday cup chamber was an absorber-foil changer consisting of a vacuum chamber with two twelve-position foil wheels. Each wheel was controlled independently and remotely so that suitable combinations of foils provided a means of measuring the primary cyclotron beam energy without the necessity of turning off the cyclotron. The beam range determination was made at the beginning and end of each day's run.

Further monitoring of the beam for the purpose of tuning cyclotron parameters was accomplished by the use of a NaI crystal scintillation counter (using a DuMont 6292 photomultiplier tube), placed externally to the scattering chamber at a forward angle of 20°. The signal from this monitor also could be used as a further check on the operation of the primary monitoring circuit.

C. Counter Characteristics

A triple-coincidence proportional counter telescope was used as a detector. This counter consisted of three chambers, each with a sensitive volume one-half inch deep and approximately two square inches in area. Each chamber contained one central ground wire and

two collector wires at positive high voltage; all wires were of 3-mil polished stainless steel.

Each counter chamber was individually tested in a constant-flow test chamber with a mixture of $A-CO_2$ gas in proportions of 96% to 4%, which was further purified by passing through a copper cooling-coil system immersed in a slush of dry ice and acetone.

The results of the counter tests indicated that within a circle 1.5 inches in diameter, centered on the counter, the pulse-height distribution at any given point varied from 6% to 8% full width at half-maximum, whereas the peak pulse height varied from point to point by ±3% from the average. The "fold" of these distributions gives a Gaussian distribution with width at half-maximum of 10.4%.

For purposes of testing and calibration, three Cm^{242} alpha sources were located on the side of the counter vacuum cover, separated from the sensitive volume by 0.25-mil aluminum foils. A remotely controlled sliding shutter, moved by means of small solenoids, was installed between sources and foil so that the pulses obtained might be observed at will. Because of their location, the pulse-height distributions from these sources had a low-pulse tail, but their mean pulse height could be used for a relative measure of counter characteristics as a function of time during a run, as well as for prerun testing of counting equipment.

Because the proportional counter was to be used in a long-range program for the detection of alpha particles, deuterons, protons, and possibly other charged particles, its pulse-height distribution characteristics were of particular interest. Pulse-height distributions of from about 10% to 15% (Fig. 2) have been observed for 48-Mev alpha particles, for settings of discriminator bias below the "knee" of the bias curves. The "width" of the pulse-height distribution is that pulse-height interval which contains one-half the observed pulses, as defined by Rossi and Staub.[6]

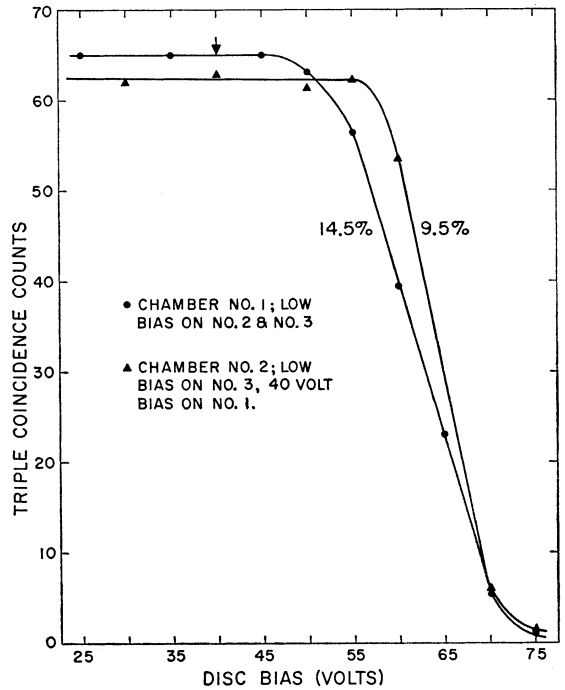

FIG. 2. Integral pulse-height distribution curves obtained with the proportional counter telescope.

For particles detected in the counter, the ratio of pulse heights in the first chamber for deuterons *versus* protons should be about 1.3, and for alpha particles *versus* protons, about 4.

A block diagram of a typical electronics setup is shown in Fig. 3.

Nominally square, delay-line-clipped counter pulses of 1 microsecond duration were used, with a rise time of about 0.2 microsecond. Preamplifiers, suspended from the bottom of the scattering chamber, provided a gain of about 75 to the linear amplifiers. This increased gain (at some small sacrifice of pulse rise time) was introduced in order to avoid high counter voltages.

Jitter in the formation of the variable gates as a result of electronics effects and of differences in electron collection time in different counter chambers was less than 0.5 microsecond. Counting rates were always determined by finding the extent of the beam plateau (region in which counts per given value of integrated beam as a function of beam intensity remained essentially constant). In this way, loss of counts because of dead time in counter and discriminators, or loss of register counts in the scalers, was avoided.

D. Measurement of the Angular Distributions

The elastic alpha particles were detected in the following manner: At some convenient angular setting of the counter telescope, sufficient absorber was inserted so that the elastic alpha particles stopped in a given counter chamber, say No. 1 (see Fig. 4). The counter voltage and the amplifier gain for that chamber were set for pulses which just reached saturation without overloading. This procedure was repeated for each of the other chambers. Discriminator curves were run for the

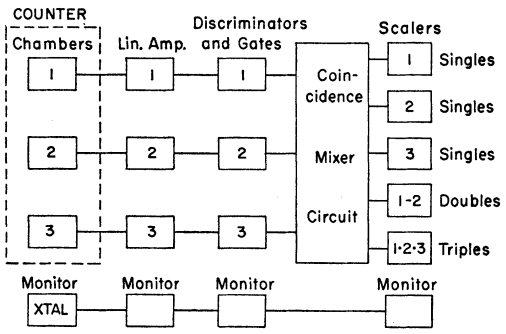

FIG. 3. Block diagram of the electronics.

[6] B. B. Rossi and H. H. Staub, *Ionization Chambers and Counters, Experimental Techniques* (McGraw-Hill Book Company, Inc., New York, 1949), p. 96.

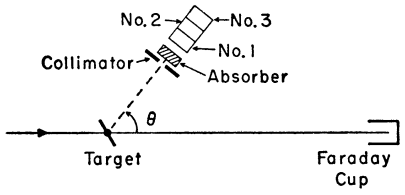

FIG. 4. Schematic diagram of the counter arrangement.

pulses from each of the chambers at an absorber setting 20 mg/cm² below the value that had produced the peak pulse heights. The biases were then set so that chambers No. 1 and No. 2 could detect an alpha particle with 20 mg/cm² of residual range or less. Chamber No. 3 had its bias set very low, so that it could detect any pulse above the amplifier noise. The coincidence circuits monitored both 1–2 coincidences (doubles) and 1–2–3 coincidences (triples). Differential range spectra were run by plotting doubles minus triples against absorber thickness for a fixed amount of collected charge in the Faraday cup. The elastic peak showed up well, and its width could be accounted for by the spread in incident beam energy, range straggling, and the target thickness. At absorber settings just below the peak, the doubles rate is essentially flat, and represents the integral of the differential elastic peak. The desired angular distributions, then, were made by measuring these double coincidences as a function of angle, normalized to the charge collected by the Faraday cup. Each point was multiplied by $\sin^4(\theta/2)$ to give the ratio to Coulomb scattering. Good reproducibility was observed from run to run, and many of the data were run several times in order to verify structure in the distributions. Runs at different beam levels or between different angular regions always included overlapping measurements, to insure that no large error in normalization remained undetected.

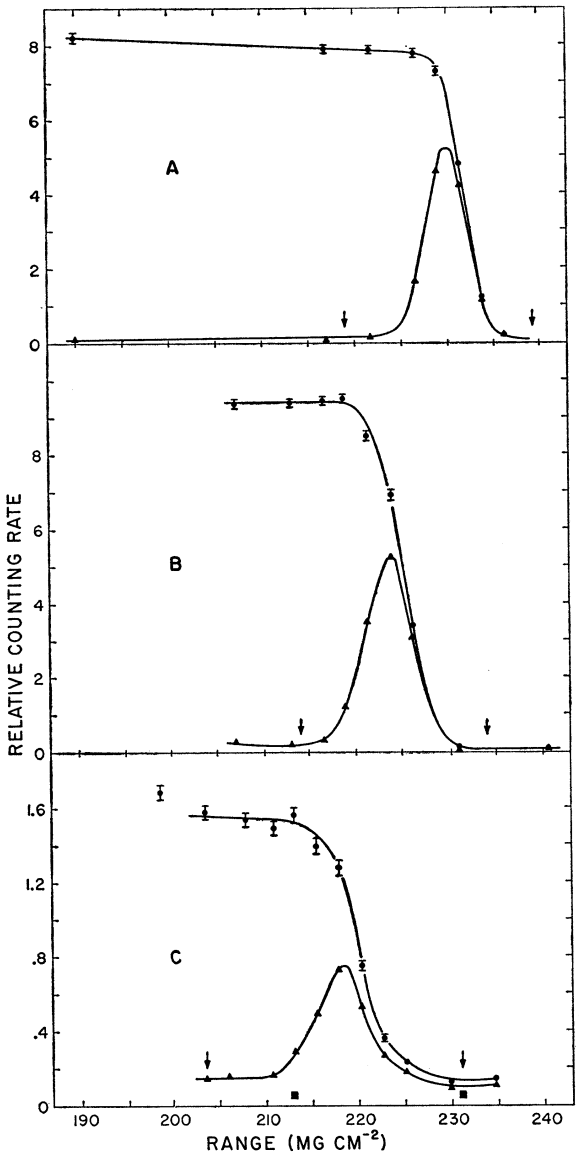

FIG. 5. Typical integral and differential range spectra. 5*A* is for Au at 45°, 5*B* is for Ag at 30°, and 5*C* is for Pb at 75°. The dark squares in 5*C* represent the differential target-out background.

It was, of course, also possible to integrate numerically the differential spectrum at each angle. Comparison of the two methods always gave very good agreement for a reasonable value of the range "bite" of the counter (the thickness of the range foil plus about one-half the thickness of the second chamber, depending on bias settings in the second and third counter chambers).

The differential spectrum was run at angles up to 75° in making this check. The good agreement between the differential and integral method gave confidence that the quantity being measured was actually the elastic scattering cross section. Typical curves of the integral and differential spectra are shown in Fig. 5.

E. Background

At each angle, data were taken with the target out, to account for background. At regular intervals complete differential range spectra were run in order to determine the background level. It turned out that the background was insignificantly low at angles out to 50°. Beyond, the elastic peak was found with a general background of charged particles which appeared at absorber values both above and below that of the elastic alpha particles. For the wider angles, the doubles rate was determined both immediately above and below the elastic peak for target out and target in, and this background was taken into account.

To reduce background at the chamber, the three carbon beam collimators, located at the scattering chamber, were removed. Adjustable carbon slits on the cyclotron side of the strong-focusing magnet (see Fig. 1) were set to 0.3 inch. This markedly reduced both the target-out-background as well as the target-in doubles count above the elastic peak. The strong-focused beam was then 0.25 inch in diameter at the target position. All

the data on Pb were run without the chamber collimators, and for forward angles, the adjustable carbon slits, just before the strong-focusing magnet, were closed to about 0.05 inch.

One possible source of error might have arisen if inelastic alpha particles with small energy losses were counted in significant numbers. It is not likely that this happened, since the observed data fitted the Coulomb scattering at the forward angles (up to 20°) and there was essentially no such background in plots of the differential spectra.

A calculation indicates that alpha particles scattered elastically from any residual carbon or oxygen on the targets would not be detected beyond about 15°. Between 7° and 15° any such contaminant effect would be small compared with the large cross section of the target.

F. Resolution

The cyclotron beam was collimated by means of adjustable carbon slits to less than 0.3 inch in width before it entered the strong-focusing lens system. When focused at the target position in the usual 0.25-inch-diameter spot, it was considered to be a parallel beam of particles. Because the target was always maintained at 45° to the plane perpendicular to the beam direction, the scattered particles emerged from an elliptical spot. When multiple scattering in the target, the size and shape of the target spot, and the size of the counter collimator were taken into account, the angular resolution was determined by a fold of the functions representing these quantities. The width at half-maximum was ±1° for the least favorable case in which a Pb target was bombarded without the one-eighth-inch carbon collimators mounted in the beam duct just outside the scattering chamber.

G. Estimate of Error

The ratio σ/σ_c of the observed differential cross section to the Coulomb cross section, as a function of the scattering angle, was the experimental quantity of interest here. The yield of counts per microcoulomb of integrated beam at a given angle was normalized to the smallest angle at which reliable data were obtained and the ratio σ/σ_c was taken to be unity at that angle.

In determining these quantities, the scaler reading and pen-recorder reading of the voltage across the precision capacitor used with the integrating electrometer were made. It was estimated that the values of the capacitors were known to within 1% and the uncertainty in recorder readings to within 0.5%. The fractional standard deviation in counts, with background taken into consideration, was combined quadratically with the fractional standard deviation of the value of the integrated beam to obtain the uncertainty in σ/σ_c.

As an example, the magnitude of the uncertainty in σ/σ_c for Au at 45°, normalized at 7° (laboratory system) yields a fractional standard deviation of 2.1%.

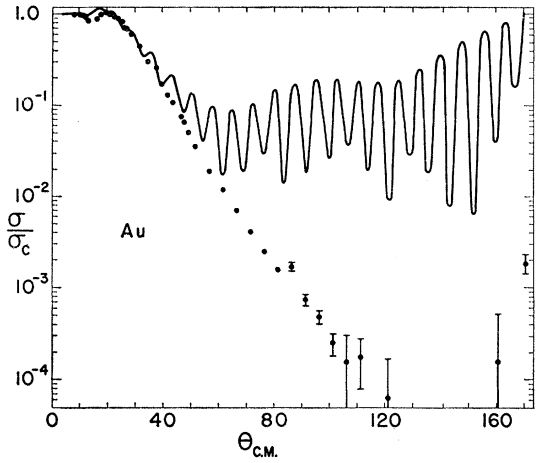

FIG. 6. The angular distribution of 48-Mev alpha particles scattered elastically from Au. The solid curve represents the best fit according to the modified Blair theory. Angles are in degrees.

The uncertainties, both with respect to the scattering angle and the ratio σ/σ_c, lie essentially within the area of the circular dots or otherwise indicated limits of uncertainty as shown in the angular distributions.

III. RESULTS

The angular distributions obtained with 48.2-Mev alpha particles elastically scattered from Au, Pb, and Ag are shown in Figs. 6, 7, and 8. The curves shown are theoretical and were derived from the application of a modification of Blair's theory, to be discussed below.

The data for Au show that the cross section dips below and then rises about 3% above that for Coulomb scattering at 20°, and then falls exponentially, with slight indications of some structure at 38°, 48°, and 88°. Beyond 100° the cross section is $\sim 10^{-4}$ that for Coulomb scattering. Points were taken every 10° between 120° and 160°, which all lie below the indicated

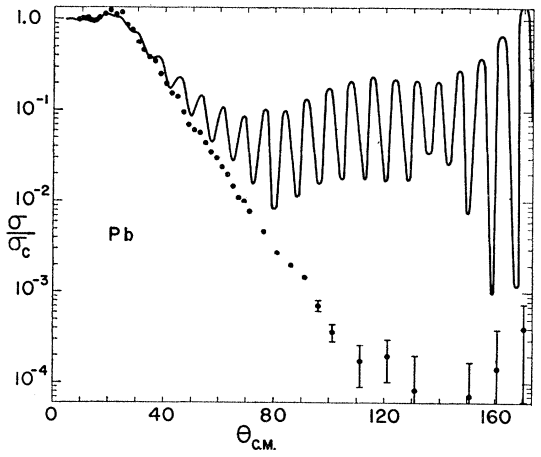

FIG. 7. The angular distribution of 48-Mev alpha particles scattered elastically from Pb. The solid curve represents the best fit according to the modified Blair theory. Angles are in degrees.

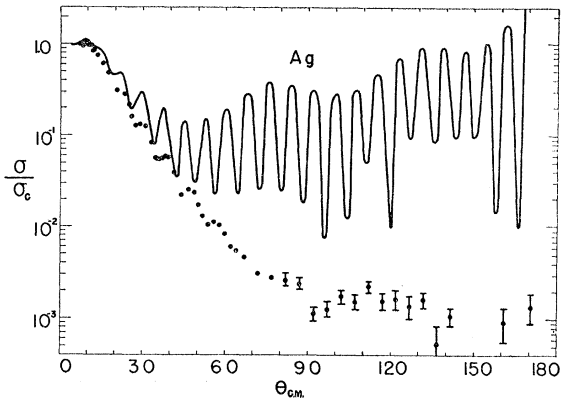

FIG. 8. The angular distribution of 48-Mev alpha particles scattered elastically from Ag. The solid curve represents the best fit according to the modified Blair theory. Angles are in degrees.

ordinates. The points at 160° and 170° indicate a possible rise in the extreme backward direction.

The data for Pb show a similar general behavior, but the maximum rise is to 26% above Coulomb scattering at 20° and definite diffraction maxima may be seen at 38°, 45°, 53°, 70°, and 90°. The point at 140° lies below 10^{-4}, and beyond 150° a slight rise in the cross section appears.

The data for Ag show a 2% rise above Coulomb at 10° and the falloff shows a regular diffraction pattern with distinct maxima at 24°, 30°, 39°, 47°, and 56°. Beyond 90° the cross section remains near 10^{-3} that for Coulomb scattering, except for the lower point at 150°.

IV. THEORY AND DISCUSSION

A. The Modified Blair Theory

The sharp diffraction patterns and relatively high cross sections predicted by Blair's theory, as described in Sec. I, were not observed in these data. On the assumption that this effect is due to the sharp radial cutoff of the theory, it was decided to extend the modification suggested by Wall *et al.* by weighting the partial-wave amplitudes in such a way as to introduce a broad transition region of interaction. Since, from Eq. (2), $l'=f_1(R)$, then $\Delta l'=f_2(l',R)\Delta R$. Here ΔR represents a region in which the nuclear density is falling off and has been taken to be equal in magnitude to the alpha-particle radius. Over this region the absorption has been made to decrease linearly. Elsewhere $W_l=1$ (complete absorption) for $l\leqq l'-\Delta l'$, and $W_l=0$ (no absorption) for $l\geqq l'$. W_l is shown as a function of l/l_{c1} in Fig. 9. The sharp cut-off model and Wall's modification are shown for comparison. The target elements and alpha-particle energy in this experiment yield a transition region whose magnitude is given by $\Delta l'/l'\sim\frac{1}{3}$, or alternatively, $\Delta R/R\sim\frac{1}{4}$.

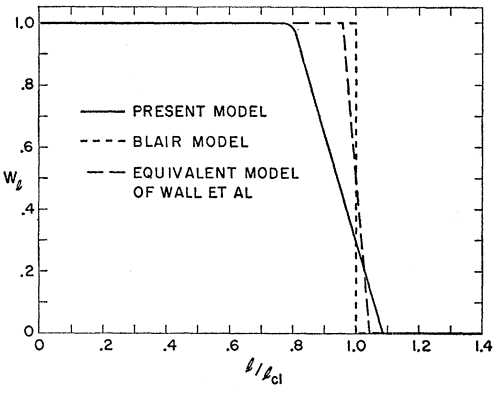

FIG. 9. The weighting factor W_l for removing the lth partial wave as a function of l/l_{c1}. Here l_{c1} is the value of l' that results from Eq. (2).

In general the introduction of a relatively large transition region causes the theoretical distributions to fall off somewhat faster. The diffraction pattern, however, still appears with the large oscillations characteristic of the sharp-cutoff theory. For the forward angles the curves agree qualitatively with the observed distributions and are sufficiently sensitive to choice of l' that they may be used to determine interaction radii by fitting the curves to the data. Figure 10 shows the effect of changing l' by a small amount. The curves fall more sharply with increasing l'. Figure 10 also compares modified theoretical distributions with a sharp-cutoff distribution for the same target. The modified distribution can be characterized by the parameter l_{max}', the value of l' for which W_l approaches zero. If the data are fitted with both modified and sharp-cutoff theories, the value of l_{max}' for the modified theory is somewhat larger than the l' for the sharp-cutoff model. Then l_{max}' corresponds to a maximum interaction radius. The fact that even the modified distributions do not drop sharply enough and contain large oscillations is perhaps evidence

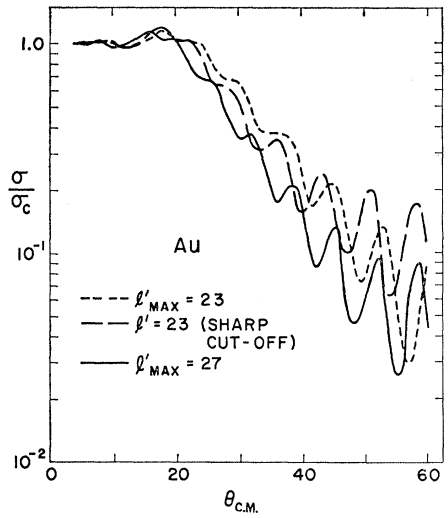

FIG. 10. The dependence of the angular distribution on the value of l_{max}'. Angles are in degrees.

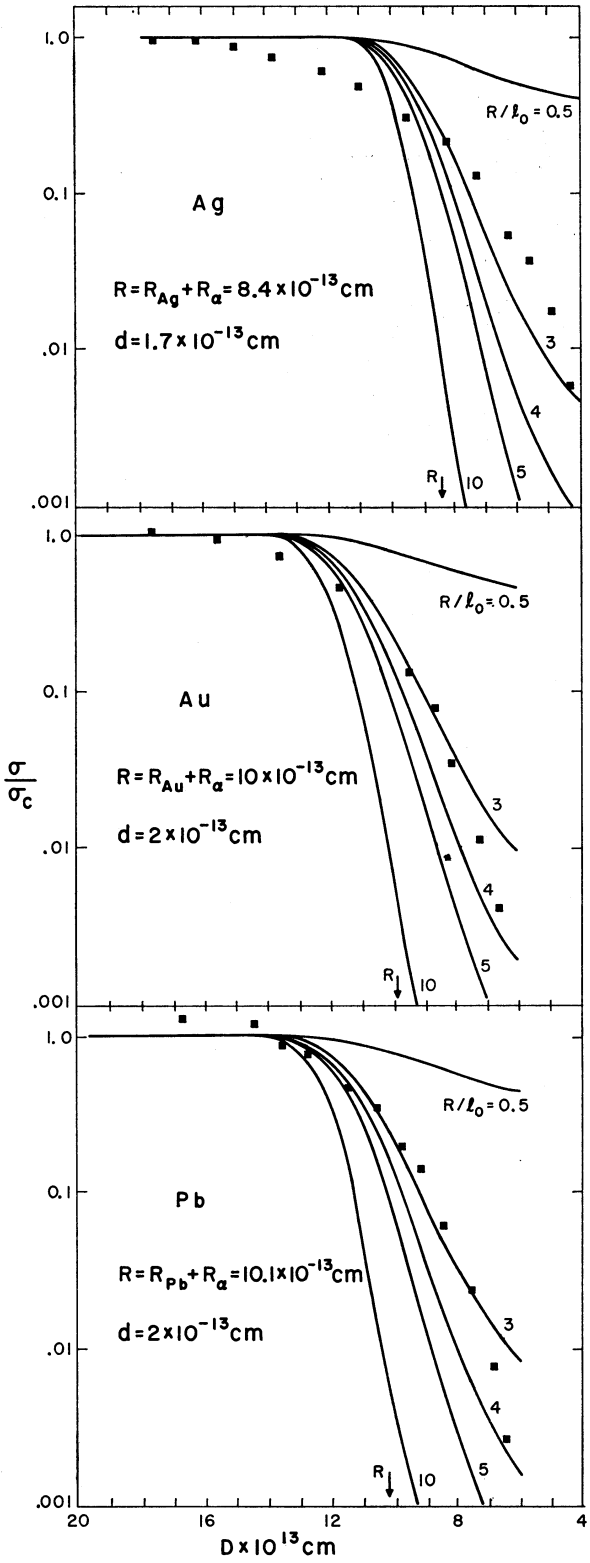

FIG. 11. The angular distributions as a function of D, the apsidal distance, according to Porter's theory. Only a limited number of experimental points are included.

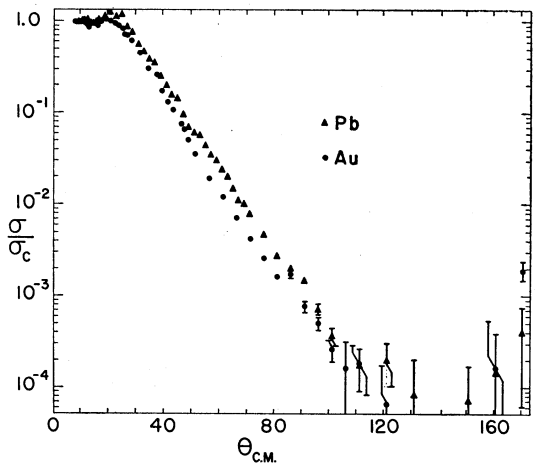

FIG. 12. The angular distributions for Pb and Au plotted together for comparison. Angles are in degrees.

that a yet larger transition region is required, in contrast with the results at 22 Mev.

B. The Porter Theory

Shown in Fig. 11 are plots of the ratio of observed to Coulomb cross section as a function of the apsidal distance D according to Porter's theory.[6] The curves are those contained in his work and the values of D shown there do not extend to the higher values (up to $D\sim40\times10^{-13}$ cm) that would be necessary for the scattering at angles less than about 15° for Pb or Au bombarded with 48.2-Mev alpha particles.

Choosing $R=R_n+R_\alpha$, with $R_n=1.5A^{\frac{1}{3}}\times10^{-13}$ cm and $R_\alpha=1.2\times10^{-13}$ cm, we find that the theory reproduces the general features of the data but that the comparison does not yield unique values of the parameters d and R/l_0, which are varied to obtain the curves shown. For Pb and Au, the diffuseness parameter $d=2\times10^{-13}$ cm is a reasonable choice and $R/l_0\sim3$ or 4 gives best agreement. For Ag, the best value of R/l_0 is more uncertain than for Au and Pb, since none of the curves fits the data closely.

TABLE I. Interaction radii for 48.2-Mev elastically scattered alpha particles. Method A is the Blair one-quarter-point formula. Method B is the fitting of the modified Blair theory to experimental data. Method C is the fitting of the Ford-Wheeler theory to experimental data.

	E_α (Mev)	Method	$R=R_n+R_\alpha$ Ag	Au	Pb
Washington[a]	13 to 42	A	8.3 ±0.3	10.05±0.16	10.26±0.17
		A		10.45±0.25	
Indiana[b]	22	B	9.9	11.1	11.4
		A	9.1 ±0.3		
Brookhaven[c]	40	B	9.1	10.7	10.9
		C	8.69	10.06	10.20
Berkeley	48.2	A	8.35±0.28	10.04±0.20	10.01±0.19
		B	9.41±0.17	10.5 ±0.2	10.3 ±0.2

[a] See reference 3.
[b] See reference 5.
[c] See reference 7.

TABLE II. Determination of $\Delta R = R_{Pb} - R_{Au}$, in units of 10^{-13} cm. θ_{Au} = angle of scattering from Au nucleus in degrees. θ_{Pb} = angle of scattering from Pb nucleus for which $\sigma/\sigma_c(\text{Pb},\theta_{Pb}) = \sigma/\sigma_c(\text{Au},\theta_{Au})$. $\Delta\theta = \theta_{Pb} - \theta_{Au}$.

θ_{Au}	$\Delta\theta_{exp}$	$\Delta R=-0.15$	$\Delta R=-0.10$	$\Delta R=-0.05$	$\Delta R=0$	$\Delta R=0.05$	$\Delta R=0.10$	$\Delta R=0.15$	$\Delta R=0.20$	$\Delta R=0.25$
25	3.3	1.6	1.4	1.3	1.2	1.1	0.9	0.8	0.7	0.6
30	2.5	2.0	1.8	1.7	1.5	1.3	1.1	0.9	0.8	0.6
45	2.5	3.8	3.4	3.0	2.5	2.1	1.7	1.3	0.9	0.6
60	5.5	6.2	5.4	4.6	3.8	3.1	2.3	1.5	0.9	0.6
75	5.5	11.7	10.2	8.6	7.4	6.1	4.8	3.6	2.4	1.2
90	4.0	14.5	12.2	9.9	7.9	5.9	4.3	2.3	0.5	···
100	4.0	19.1	15.7	12.7	10.0	7.3	4.8	2.5	0.3	···
120	20	39.7	29.7	22.5	16.4	11.5	7.1	3.0	···	···

C. Interaction Radii

Values of the interaction radii have been estimated from these data by (*a*) using the modified version of Blair's theory to obtain the value of l' for which a best fit is obtained and solving for R in Eq. (2); and (*b*) using Blair's result that for a given alpha-particle energy the value of the scattering angle θ, for which the ratio $\sigma/\sigma_c = \frac{1}{4}$ yields R from the equation for the apsidal distance $D_{1/4} = R = (2Ze^2/2E)[1+\csc(\theta_{1/4}/2)]$. Table I lists interaction radii obtained by these methods. The results of other experiments are included for comparison.

The nominal values indicate that the interaction radius for Pb may be slightly smaller than that for Au, in contrast to the results of other experimenters. This may be evidence of a closed-shell configuration in Pb, but the uncertainty in curve-fitting and in normalization are sufficiently large that this effect is in doubt. The values obtained here seem to be in general agreement with the other results.

The angular distributions for Au and Pb are very similar, qualitatively. Both sets of data are plotted together in Fig. 12. Wall *et al.*[3] have explained a similar result obtained at 22 Mev using a classical interaction model in which the angular distribution depends only on the distance between the alpha particle and the nuclear surface. Under the same assumptions, these data were analyzed to obtain $R_{Pb} - R_{Au}$, and the results (shown in Table II) yield no consistent pattern. The displacement of the two curves, instead of being a smooth function of the angle θ, varies from point to point because of differences in the details of structure in the two distributions. The failure is probably—at least partially—because the criterion for the classical approach, $n \gg 1$, is not well satisfied for $n \sim 7$. An alternative explanation is that the assumptions concerning the interaction are not correct at 48 Mev.

TABLE III. Interaction radii computed from various formulas; R_1 using $1.5A^{\frac{1}{3}}$, R_2 using $1.22A^{\frac{1}{3}}+0.7$, and R_3 using $1.33A^{\frac{1}{3}}$. R_4 and R_5 were determined from this experiment by methods A and B, respectively. The alpha-particle radius in each case was computed by the same formula as the nuclear radius. All radii are in units of 10^{-13} cm.

	$R_j = R_n + R_\alpha$				
Element	R_1	R_2	R_3	R_4	R_5
Ag	9.52	9.15	8.44	8.35	9.41
Au	11.11	10.44	9.85	10.04	10.5
Pb	11.27	10.57	9.99	10.01	10.3

The elastic scattering of medium-energy nucleons has recently been analyzed by several investigators.[7,8] Application of the optical model of the nucleus shows that the parameter representing the nuclear radius has nearly the same value over a wide range of elements. Several of these values have been used to compute interaction radii to be compared with the radii determined from the data. The results are shown in Table III. The interaction radii determined by method A agree most closely with a nuclear radius given by $R_n = 1.33A^{\frac{1}{3}} \times 10^{-13}$ cm, while the radii determined by method B agree best with $R_n = (1.22A^{\frac{1}{3}}+0.7)\times 10^{-13}$ cm.

Preparations have been made to submit the data for analysis on the optical model theory. If the experimental data can be fitted over a wider range of angles by this method, more accurate values of the nuclear parameters that characterize the scattering can be obtained.

V. ACKNOWLEDGMENTS

It is a pleasure to thank Professor A. Carl Helmholz and Dr. C. M. Van Atta for their interest and support. Dr. Warren Heckrotte has provided many valuable discussions concerning the experiment. Dr. Sidney Fernbach has contributed invaluable time and effort in the Univac program which made the many laborious computations possible. The assistance of Mr. Frank Vaughn, Mr. Homer Conzett, and Mr. Robert Summers-Gill in setting up the cyclotron runs and obtaining the data is gratefully acknowledged. Mr. G. Bernard Rossi, Mr. William B. Jones, and the other members of the 60-inch cyclotron group have provided outstanding cyclotron operation for all the runs.

[7] Melkanoff, Nodvik, Saxon, and Woods, University of California at Los Angeles Technical Report 7-12-55, (unpublished).
[8] S. Fernbach (private communication).